JACS
JOURNAL OF THE AMERICAN CHEMICAL SOCIETY
pubs.acs.org/JACS

Open Access
This article is licensed under CC-BY-NC-ND 4.0

Article

High-Resolution Multicolor Shortwave Infrared Dynamic *In Vivo* Imaging with Chromenylium Nonamethine Dyes

Anthony L. Spearman, Eric Y. Lin, Emily B. Mobley, Andriy Chmyrov, Bernardo A. Arús, Daniel W. Turner, Cesar A. Garcia, Kyle Bui, Christopher Rowlands, Oliver T. Bruns, and Ellen M. Sletten*

Cite This: *J. Am. Chem. Soc.* 2025, 147, 17384−17393

Read Online

ACCESS | Metrics & More | Article Recommendations | Supporting Information

ABSTRACT: Imaging in the shortwave infrared (SWIR) region offers fast, high-resolution visualization of *in vivo* targets in a multiplexed manner. These methods require bright, bathochromically shifted fluorescent dyes with sufficient emission at SWIR wavelengths—ideally above 1500 nm for high-resolution deep tissue imaging. Polymethine dyes are a privileged class of contrast agents due to their excellent absorption and high degree of modularity. In this work, we push flavylium and chromenylium dyes further into the SWIR region through polymethine chain extension. This panel of nonamethine dyes boasts absorbances as red as 1149 nm and tail emission beyond 1500 nm. These dyes are the brightest organic fluorophores at their respective bandgaps to date, with $\varepsilon_{max} \sim 10^5$ M^{-1} cm^{-1} and Φ_F up to 0.5%. Using two nonamethine dyes, **Chrom9** and **JuloFlav9**, we performed two-color all-SWIR multiplexed imaging (Excitation at 1060 and 1150 nm; Emission collection at >1500 nm), enhancing the depths and resolutions able to be obtained in multicolor SWIR imaging with small molecule contrast agents. Finally, we combine the nonamenthine dyes with other SWIR-emissive fluorophores and demonstrate five-color awake imaging in an unrestrained mouse, simultaneously pushing the multiplexing, resolution, and speed limits of *in vivo* optical imaging.

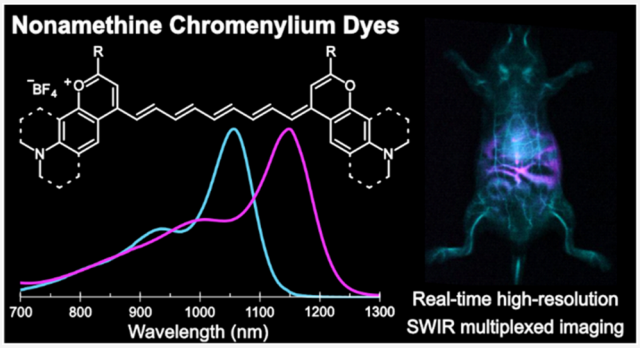

INTRODUCTION

Multiplexed optical imaging is a ubiquitous approach to real-time studies of dynamic biological processes in cells and transparent organisms. Considerable progress toward bringing the advantages of optical imaging to mammals has been achieved by leveraging the shortwave infrared (SWIR, 1000−2000 nm, Figure 1A) region of the electromagnetic spectrum.[1−5] The SWIR region increases opportunities for multiplexed imaging in mammals by expanding wavelengths compatible with imaging through tissue from a few hundred nanometers in the near-infrared (NIR, 700−1000 nm) region to over 1000 nm, if the entire SWIR region can be utilized.[6] Additionally, the SWIR region can provide higher resolution imaging at greater depths as a result of the decreased scattering of long wavelength light by tissue and minimal autofluorescence.[7,8] However, not all regions of the SWIR display equivalent properties.[9] The major advantages of the SWIR region become especially apparent when imaging in the water absorption band (i.e., 1350−1450 nm) to achieve exceptional resolution,[10,11] or imaging above 1500 nm where depths upward of 0.5 cm can be obtained while maintaining superior resolutions.[12,13]

Hundreds of small molecule fluorophores have been developed for imaging above 1000 nm since the seminal report of SWIR (also called NIR-II) imaging in 2009;[5] yet, the majority of these fluorophores are only able to be detected at real-time speeds at wavelengths in the first portion of the SWIR region (i.e., 1000−1300 nm) where only subtle improvements over the NIR are achieved.[12,14] The lack of small molecule fluorophores for real-time imaging above 1300 nm stems from brightness limitations due to the energy gap laws that severely limit quantum yields as the λ_{max} is bathochromically shifted within the SWIR region.[15,16] To date, there are only a handful of reports of single-color video-rate imaging above 1350 nm.[17−20]

Ultimately, a significant advantage of the SWIR region is dynamic multiplexed imaging. For multiplexed imaging in real-time, the brightness requirements for fluorophores are more

Received: March 5, 2025
Revised: April 10, 2025
Accepted: April 14, 2025
Published: May 9, 2025

ACS Publications
© 2025 The Authors. Published by American Chemical Society

https://doi.org/10.1021/jacs.5c03673
J. Am. Chem. Soc. 2025, 147, 17384−17393

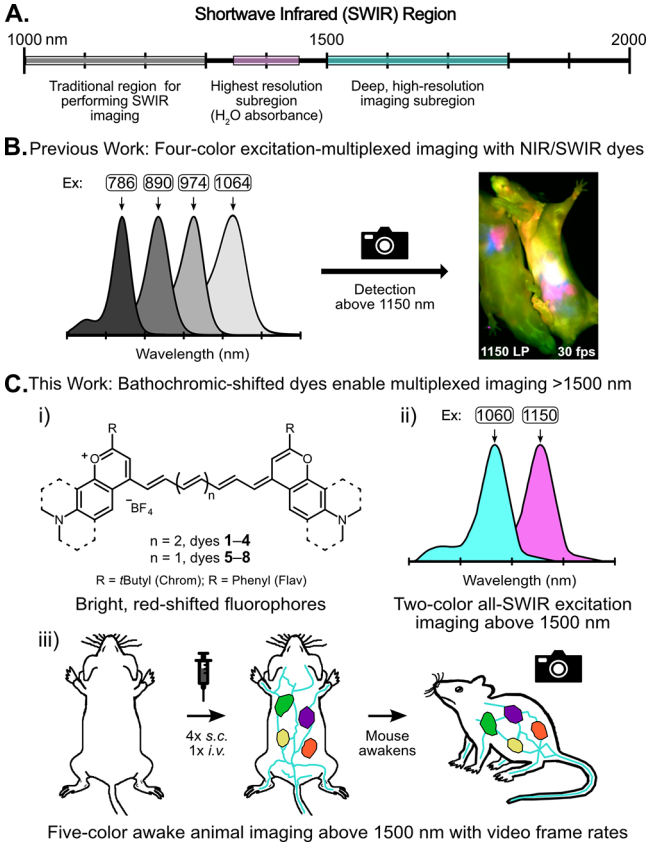

Figure 1. (A) Subregions of the shortwave infrared region of the electromagnetic spectrum and their utility for fluorescence imaging. (B) Previously reported four-color excitation multiplexed imaging strategy in the traditional SWIR imaging window. Image reproduced from ref 23. Available under a CC-BY 4.0 license. Copyright 2023 Arús, Cosco, Yiu, Balba, Bischof, Sletten and Bruns. (C) Herein, Chromenylium-based dyes (i) allow for the first example of all-SWIR excitation-multiplexed imaging (ii) and five-color awake imaging with video frame rates (iii).

stringent as imaging speeds are divided by the number of channels. Using an excitation-based approach to multiplexing,[21] we have previously been able to perform four-color, real-time imaging in mice using three NIR dyes (**ICG**, Ex = 785 nm; **JuloChrom5**, Ex = 890 nm; **Chrom7**, Ex = 980 nm) and one SWIR dye (**JuloFlav7**; Ex = 1064 nm) and collection with an 1150 nm long-pass (LP) filter.[22] We were even able to perform these multiplexed experiments in awake animals, enabling organ tracking and contact-free telemetry (Figure 1B).[23] However, we were unable to obtain video-rate multiplexed images in the advantageous regions above 1350 nm.

Here (Figure 1C), we report the first all-SWIR excitation-multiplexed imaging experiment with 1060 and 1150 nm excitation and emission collection above 1500 nm at video-rate speeds. True SWIR excitation-multiplexed imaging with detection above 1500 nm enables all the advantages of the SWIR (high resolution, greater depths, multiple channels) to be capitalized upon. Additionally, we report five-color multiplexed imaging on both anesthetized and awake animals. These multiplexed imaging advances necessitated new SWIR fluorophores which were lower in energy than previously prepared flavylium dyes, and brighter than existing fluorophores available for excitation above 1060 nm. We achieved contrast agents which met these requirements by extending the polymethine chain of flavylium and chromenylium dyes and report four bright nonamethine dyes, **1**–**4**, with SWIR absorption and 100% SWIR emission. These fluorophores are the brightest organic dyes at their respective bandgaps, with $\varepsilon_{max} \sim 10^5\ M^{-1}\ cm^{-1}$ and Φ_F up to 0.5%. The lowest (**4**, named **JuloFlav9**) and highest (**1**, named **Chrom9**) energy nonamethine dyes are sufficiently spectrally separated for multiplexed imaging. This work also required the introduction of an 1150 nm laser to the excitation-based imaging setup, highlighting the complementarity of chemistry and technology improvements that have been necessary for the advancement of SWIR imaging.

RESULTS AND DISCUSSION

SWIR Fluorophore Design. To achieve multiplexed imaging in the high-resolution regions of the SWIR with organic contrast agents, fluorophores must be bright, spectrally separated, contain 100% SWIR emission, and be bathochromically shifted as much as possible. Approaches to bathochromically shift NIR polymethine dyes, such as the FDA-approved **ICG**, into the SWIR region have included polymethine chain elongation or heterocycle modification. Toward the former, extension of the polymethine chain by one C_2H_2 unit reliably imparts a ∼100 nm wavelength red-shift.[24,25] This approach has been less frequently applied toward SWIR fluorophores as extension above seven methines (i.e., heptamethine dyes) often leads to electronic ground state desymmetrization, which decreases contrast agent brightness.[26] Recently, Schnermann and co-workers have reported indolene-containing nonamethine dyes for SWIR tail imaging, and Jin and co-workers have prepared nonamethine and undecamethine variants of **ICG**, deemed **ICG-C9** and **ICG-C11**.[27−29] **ICG-C11** has an impressive fluorescence quantum yield (Φ_F) but overall moderate brightness due to its low absorption coefficient (ε_{max}), likely a result of ground state desymmetrization from polymethine chain elongation.

Heterocycle modification is a complementary strategy for bathochromic shifting. These modifications include benzannulation, tuning heterocycle electronics, heteroatom exchange or heterocycle addition.[30−35] Over the years, we have applied the strategy of heterocycle modification to produce bright, SWIR-emissive fluorophores for multiplexed imaging. These fluorophores employ chromenylium (Chrom) and flavylium (Flav) heterocycles.[21,22,36−38] Notable modifications include: (1) the addition of a julolidine moiety (Julo) to provide a ∼40 nm red-shift, (2) exchange of the 2-position phenyl group in Flav dyes for a *tert*-butyl group to give Chrom dyes that display a ∼3-fold increase in quantum yield.[22] In pursuit of fluorophores with red-shifted SWIR emission, we selected four permutations of these heterocycles: Flav (**9**), JuloFlav (**10**), Chrom (**11**), and JuloChrom (**12**) to transform into nonamethine dyes **1**–**4** (Figure 2A).

Synthesis of Nonamethine Dyes. Chromenylium and flavylium heterocycles **9**–**12** were synthesized according to previous reports (Scheme S1).[22] The heptatrienylidene benzaminium perchlorate linker **13** was achieved through a Vilsmeier−Haack reaction with **S9** followed by a condensation with aniline (Scheme S1). Finally, introduction of two equivalents of heterocycle (**9**, **10**, **11**, or **12**) with **13** in basic conditions afforded the nonamethine dyes **1**–**4**, with yields between 7−23% (Figure 2A). Careful air-free technique was required in the final condensation step to avoid oxygen-

https://doi.org/10.1021/jacs.5c03673
J. Am. Chem. Soc. 2025, 147, 17384−17393

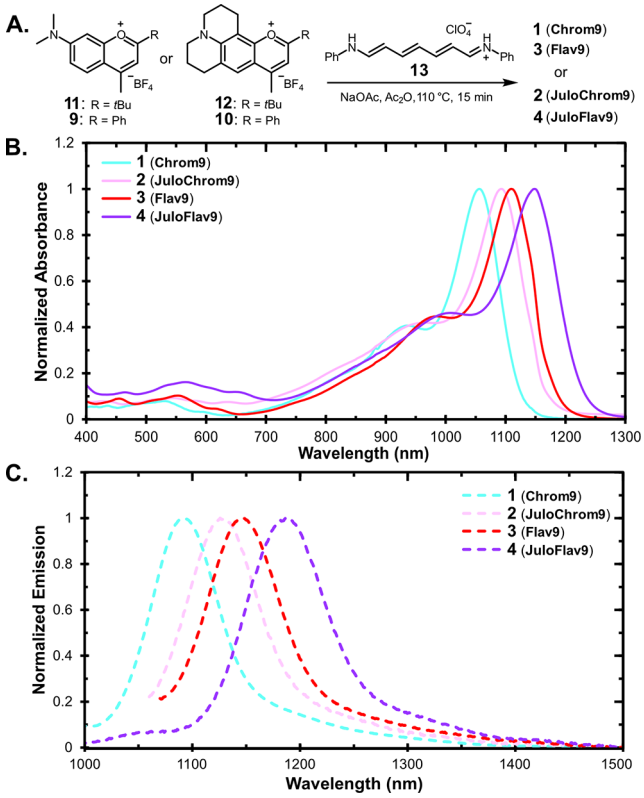

Figure 2. (A) Synthetic approach toward target nonamethine dyes **1**−**4**. (B) Normalized absorption of **1**−**4** in dichloromethane. (C) Normalized emission of **1**−**4** in deuterated dichloromethane. Emission in dichloromethane can be found in Figure S1.

mediated degradation to shorter polymethine derivatives (Figure S2). This polymethine truncation has been observed in pentamethine and heptamethine cyanine dyes.[39−41] The lower yields were attributed to a combination of truncation to shorter chain polymethine dyes and challenges with purification. Separation of the nonamethine dyes from the heptamethine and pentamethine analogues was difficult due to similar retention times.

Photophysical Properties of Nonamethine Dyes. With dyes **1**−**4** in hand, we investigated their photophysical properties in dichloromethane (Tables 1 and S1). The absorption spectra of these dyes all displayed $\lambda_{max,abs}$ above 1000 nm (Figure 2B) with $\lambda_{max,em}$ as low energy as 1188 nm (Figure 2C). The Φ_F (DCM) of these four fluorophores ranged from 0.15 to 0.5%, with the most red-shifted **4** (**JuloFlav9**) displaying the lowest Φ_F, consistent with energy gap laws.[15] Notably, three of the four fluorophores: **2** (**JuloChrom9**; $\lambda_{max,abs}$ = 1092 nm, Φ_F = 0.31%), **3** (**Flav9**; $\lambda_{max,abs}$ = 1110 nm, Φ_F = 0.19%), and **4** (**JuloFlav9**; $\lambda_{max,abs}$ = 1149, Φ_F = 0.15%), display the highest reported Φ_F at their respective wavelengths (Table 1 and Chart S1). The measured Φ_F agree with previously observed trends in that the chromenylium heterocycles result in more emissive fluorophores.

For contrast agent development, brightness is the most important comparative metric for analyzing utility for *in vivo* imaging.[6,42] Brightness is the product of ε and Φ_F, and thus a high ε can compensate for the inherently low quantum yields in the SWIR region. Fortuitously, polymethine dyes possess characteristically high ε's, rendering them excellent SWIR imaging scaffolds.[24] The ε_{max} for the nonamethine dyes **1**−**4** spanned 105,000−159,000 M^{-1} cm^{-1}, leading to brightness values of 150−540 M^{-1} cm^{-1} (Table 1). These ε_{max} values are lower than that of shorter chain chromenylium and flavylium dyes, which we attribute to the onset of ground state desymmetrization, as has been observed with other long chain polymethine dyes.[26,43] To further characterize the extent of ground state desymmetrization, absorbance in various solvents (DMSO, MeOH, acetone, and MeCN) was investigated. As expected, the dyes display more polyene-like character in polar solvents (Figure S3), which is evident in their broadened absorbance profiles. Even with some ground state desymmetrization occurring, the obtained ε values are still excellent for small-molecule dyes (~10^5 M^{-1} cm^{-1}) and result in brightness values that have previously been successful for real-time, multiplexed *in vivo* imaging with SWIR detection.[22]

Comparison of Nonamethine Dyes to Vinylene Analogues. To fully appreciate the photophysical consequences of chain extension, we directly compared the vinylene analogues derived from heterocycles **9**−**12**. Previously, we reported the direct pentamethine analogues;[27] however, our heptamethine congeners had substituted polymethine chains, precluding a direct analysis. Consequently, linear heptamethine analogues **5**−**8** were synthesized with commercially available malonaldehyde bis(phenylimine) (**S10**) using standard condensation conditions (Scheme S2). We characterized their $\lambda_{max,abs}$, $\lambda_{max,em}$, ε_{max}, and Φ_F (Table 1; errors in Table S2). These linear heptamethine dyes had $\lambda_{max,abs}$ between 935 and 1022 nm, yielding a difference in λ_{max} by about 120 nm between the 7- and 9- dyes, an observation consistent with the vinylene shift rule.[24] Interestingly, these derivatives displayed impressive Φ_F between 1.4 and 3.7%. A similar quantum yield increase has been observed with flavylium heptamethine derivatives with linear linkers.[44] These dyes had typical polymethine Stokes shifts of 26−33 nm with $\lambda_{max,em}$ as red as 1055 nm. In tandem with previous data, we can now compare the photophysical properties of 5-, 7-, and 9- linear Flav/

Table 1. Photophysical Properties of Linear Polymethine Dyes, 1−8 in Dichloromethane (DCM)

Dye	$\lambda_{max,abs}$ (nm)	$\lambda_{max,em}$ (nm)	ε_{max} (M^{-1} cm^{-1})	Φ_F (%)	Brightness (M^{-1} cm^{-1})	SWIR brightness (M^{-1} cm^{-1})
1 (Chrom9)	1057	1088	107,000	0.5	540	500
5 (LChrom7)	935	961	227,000	3.7	8400	4100
2 (JuloChrom9)	1092	1128	146,000	0.31	450	440
6 (LJuloChrom7)	970	1004	213,000	1.5	3200	1600
3 (Flav9)	1110	1133	159,000	0.19	300	290
7 (LFlav7)	986	1016	149,000	1.53	2280	1500
4 (JuloFlav9)	1149	1188	101,000	0.15	150	140
8 (LJuloFlav7)	1022	1055	212,000	1.4	3000	2800

https://doi.org/10.1021/jacs.5c03673
J. Am. Chem. Soc. 2025, 147, 17384−17393

Chrom dyes (Tables S1−S3). The λ_{max} values for the pentamethine dyes averaged 857 nm,[22,45] while those for the heptamethine and nonamethine dyes averaged 978 and 1102 nm, respectively. We then calculated the overall average brightness values to be 52,000, 4,200, and 360 M^{-1} cm^{-1} for the chromenylium penta-, hepta-, and nonamethine dyes, respectively. Notably, these chromenylium dyes show a decrease in brightness by one order of magnitude for every vinylene added to the polymethine chain, largely due to a decrease in Φ_F as predicted by energy gap laws.[15] Apart from these total brightness values, we looked to examine the brightness of each of these scaffolds in different SWIR subregions.

Considerations for SWIR Imaging. When imaging at SWIR wavelengths, the depth and resolution achievable are highly dependent on the wavelengths collected. The highest resolution images are obtained when imaging in the 1350−1450 nm region, where water absorbs scattered light, leading to high signal-to-noise ratios with mm resolution.[10,11] For high resolution with maximum depth penetration, recent works using inorganic particles have demonstrated the privileges of imaging at wavelengths above 1500 nm.[12] The wavelengths of light collected during *in vivo* imaging experiments are defined by a long pass (LP) filter, which allows only lower energy light to pass through. LP filters can modulate the balance of signal and resolution achieved. For SWIR dyes, using a 1000 nm LP filter results in all photons emitted being collected, resulting in maximum signal. Increasing the wavelength of LP filters generally leads to higher resolution images since lower energy light is scattered less by tissue and contributions from water absorption become significant above 1350 nm (Figure 3A). Therefore, imaging with 1400 nm LP or greater is preferred in order to capitalize on the advantages of the SWIR region.

To assess the potential of the chromenylium and flavylium polymethine dyes in SWIR imaging experiments with different LP filters, we first calculated their SWIR brightness by multiplying molecular brightness by their percentage of SWIR emission (1000−1700 nm; note for this analysis 1700 nm is used as the end of the SWIR region because it is the limit of the InGaAs detector). Among the nonamethine dyes, **1** (**Chrom9**) had the highest SWIR brightness around 500 M^{-1} cm^{-1} (Table 1).

We next investigated the brightness of our dyes at incrementally red-shifted LP filters, up to 1500 nm. We can determine and compare these values by preparing solutions with equal absorbance at the excitation wavelength and measuring differences in the intensity of emission as a function of LP filter. Figure 3B, 3C (1000 nm LP in Figure S4) show raw images and quantified counts of absorbance-matched **1**−**8** in capillaries under 890 nm excitation, respectively. These experiments demonstrate that despite lower Φ_F values, **4** (**JuloFlav9**), followed by **2** (**Flav9**), and **1** (**Chrom9**), are poised to yield the best images in high resolution SWIR imaging with ≥1400 nm LP filters. Notably, the high ε and Φ_F of the heptamethine dyes result in lower but still detectable signal with redder LP filters.

Micelle Formulation and Characterization. We selected **1** (**Chrom9**) and **4** (**JuloFlav9**) as the most promising nonamethine dyes for *in vivo* imaging due to their spectral separation and ability to be excited by SWIR laser lines. In preparation for animal experiments, we encapsulated the hydrophobic nonamethine dyes into amphiphilic poly(ethylene glycol)-phospholipid micelles (Figure 4A). In the micelles, the

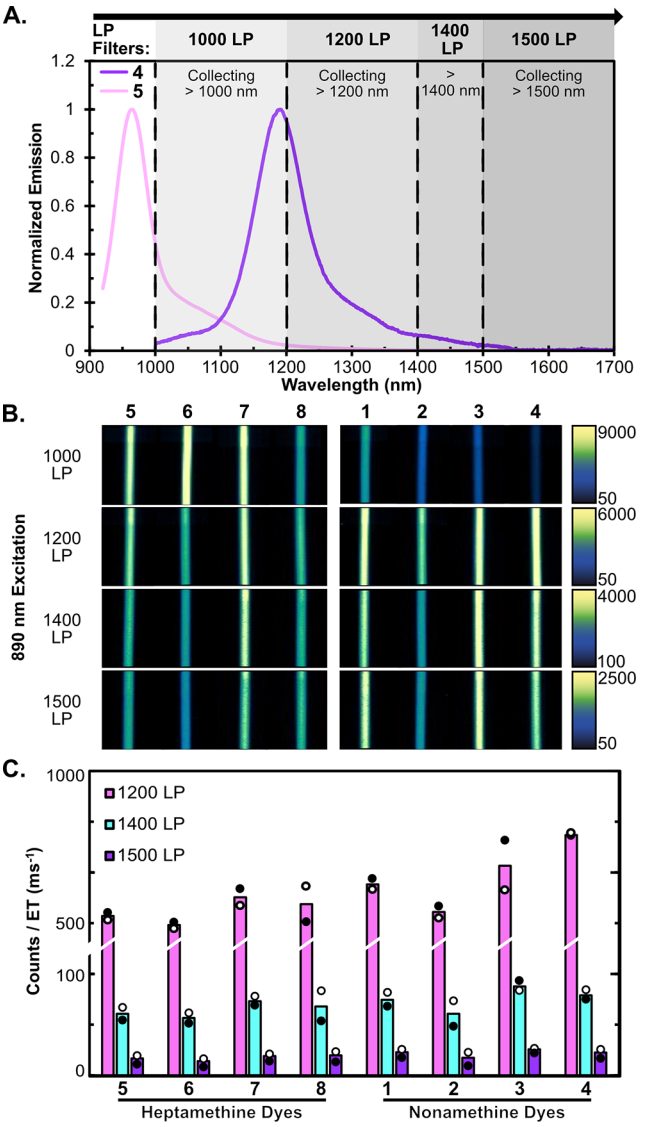

Figure 3. (A) Emission collected at different SWIR LP filters for dyes **4** (**JuloFlav9**) and **5** (**LChrom7**). (B) Capillary images of absorbance matched dyes in dichloromethane under 890 nm excitation, all with 0.7 ms ET. (C) Quantified results from capillaries in 3B, averaged over 2 trials (black and white dot denote separate trials). 1000 LP intensity is plotted in Figure S4.

nonamethine dye absorption was broadened and aggregation was observed, particularly in the **JuloFlav9** micelles (Figure S5). The micelles were approximately 17 nm in size (Figure S6, avg. number). These results are consistent with the encapsulation of previously published fluorophores, where Flav dyes displayed increased aggregation over Chrom dyes.[22] We further assayed the stability of the fluorophores within the micelles. First, we addressed their chemical stability by treating micelles containing nonamethine dyes **1** and **4**, as well as previously reported heptamethine analogues, with 1 mM lysine, tyrosine, glutathione in phosphate buffered saline (Figure S7). Good stability was observed over 24 h in all conditions. At 48 h, degradation started to be apparent, especially upon tyrosine treatment (Figure S7). The nonamethine and heptamethine dyes were both susceptible to this degradation pathway, although additional degradation produc-

https://doi.org/10.1021/jacs.5c03673
J. Am. Chem. Soc. 2025, 147, 17384−17393

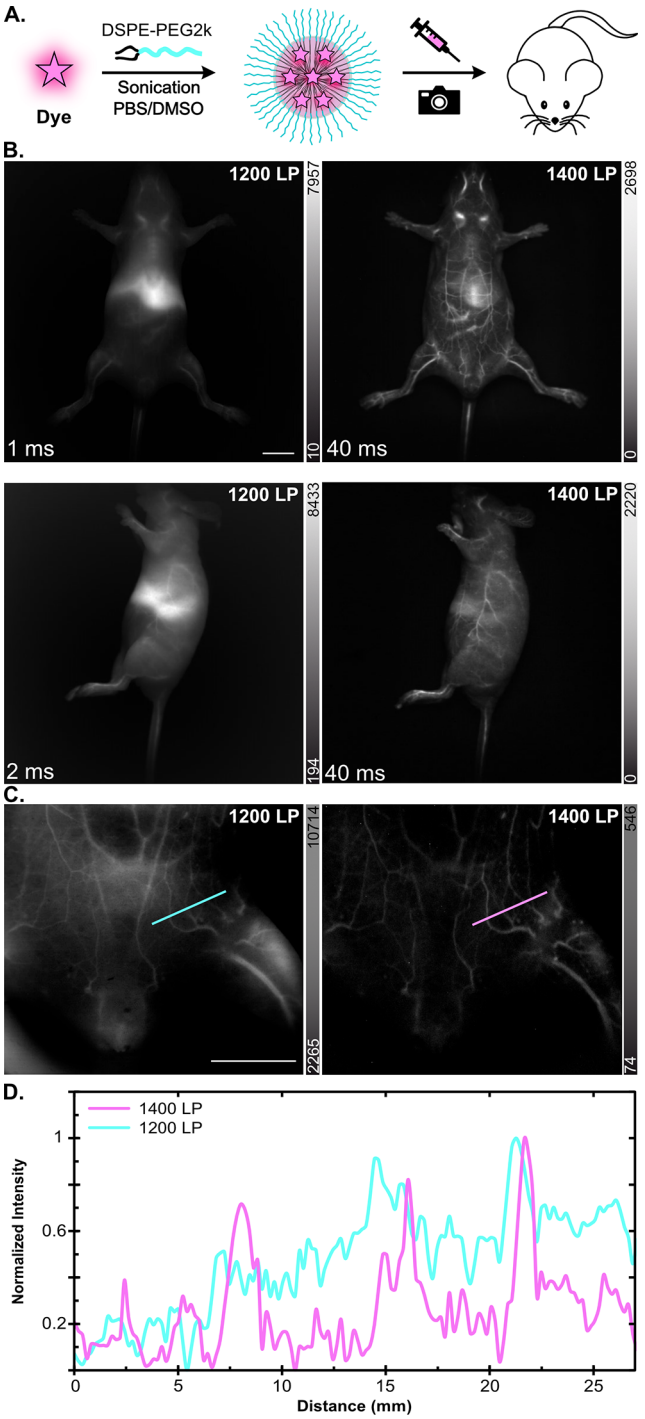

Figure 4. (A) Scheme for micelle formulation and subsequent *in vivo* delivery. (B) Vasculature imaging with **1** (**Chrom9**). ETs are as listed and scale bar = 10 mm. (C) Imaging with **1** (**Chrom9**) with zoom lens (2.5× magnification), ET = 100 ms, scale bar = 10 mm. (D) Quantification of ROI in (C). Power densities were 161 mW cm^{-2}.

ing truncation products was also observed for **JuloFlav9** (Figure S7B–D).

We evaluated the toxicity of micelles containing **Chrom9** and **JuloFlav9** *in cellulo*. A375 cells were incubated with three concentrations of **Chrom9**, **JuloFlav9**, or empty micelles and their viability after 24 h was assessed using the MTT assay (Figure S8). The viability of cells cultured with empty micelles were comparable to what was observed with **Chrom9** and **JuloFlav9** micelles, suggesting negligible toxicity.

Next, we addressed the photostability of micelles containing **Chrom9** and **JuloFlav9** compared to micelles containing **JuloFlav7**. These samples were irradiated by a 1060 nm laser for 5 min to assess the relative photostability of the novel nonamethine dyes (Figure S9). We observed similar photostability for all dye-containing micelles.

Single Color Imaging of Chrom9. With promising micelle characterization in hand, micelles containing **1** (**Chrom9**) were i.v. injected, and vasculature images were immediately acquired with 1060 nm excitation (Figure 4B). When using a 1300 nm LP filter, standard for imaging experiments with 1060 nm excitation, video-rate speeds were readily obtained (Video S1). When imaging with the 1400 nm LP filter, the enhanced resolution of this SWIR subregion was apparent, which was further highlighted when the magnification was increased (Figure 4C–D). After 1 h, **1** (**Chrom9**) was cleared from the vasculature and resided in the liver and spleen, which was confirmed at 48 h by *ex vivo* analysis (Figure S10). However, to gain greater insight into how long **Chrom9** remained in the liver *in vivo*, longitudinal imaging was performed (Figure S11). After 1 day, migration of **Chrom9** toward the liver and spleen was observed. After 4 days, a dramatic loss of signal was observed, with barely any signal at 8 days. At 16 days, organs were excised, giving hardly any detectable signal and preventing a full *ex vivo* analysis. This loss of signal is either due to clearance or degradation, which cannot be decoupled in fluorescence-based clearance studies. When considering the micelle stability studies (Figure S7), it is likely that degradation is significant at the 1-week time point, and that these probes are only applicable for imaging within ∼48 h.

Imaging with 1150 nm Excitation. With the development of **4** (**JuloFlav9**) that has a $\lambda_{max,abs}$ = 1149 nm, we desired an excitation source that was better aligned with this fluorophore to maximize absorption (Figure 5A). We expanded our excitation capabilities through the addition of a 1150 nm laser. Briefly, a 10 W 1150 nm laser from MPBC was collimated, reflected off two mirrors and then aligned through a series of achromats, short-pass filters, and diffusers (see SI for further details). After validating that **JuloFlav9** and micelle formulations of **JuloFlav9** could be visualized via excitation with the 1150 nm setup, we performed single channel vasculature imaging of **JuloFlav9** using a 1200 nm LP filter (Figure 5B). *Ex vivo* analysis after 48 h showed localization to the liver and spleen as seen with **Chrom9** (Figure S12) but with overall lower signal.

Multiplexed Experiments. **JuloFlav9** and the 1150 nm laser line provided opportunities for two new multiplexed imaging experiments: (1) all-SWIR two-color imaging with collection in the high resolution/high depth penetration SWIR subregions above 1500 nm and (2) five-color optical imaging with biocompatible probes, even in awake and unrestrained animals. We established that **Chrom9** and **JuloFlav9** in micelle formulations were able to be multiplexed using 1060 and 1150 nm excitation (Figure 5A). Upon optimization, we found that using 15 nmol of **1** (**Chrom9**) and 10 nmol of **4** (**JuloFlav9**) provided good signal from **1** (**Chrom9**) upon 1060 nm excitation and **4** (**JuloFlav9**) upon 1150 nm excitation using a 1500 nm LP filter with minimal crosstalk (Figure 5C).

Following these conditions that yielded minimal crosstalk, we performed the first all-SWIR multiplexing experiment with

https://doi.org/10.1021/jacs.5c03673
J. Am. Chem. Soc. 2025, 147, 17384–17393

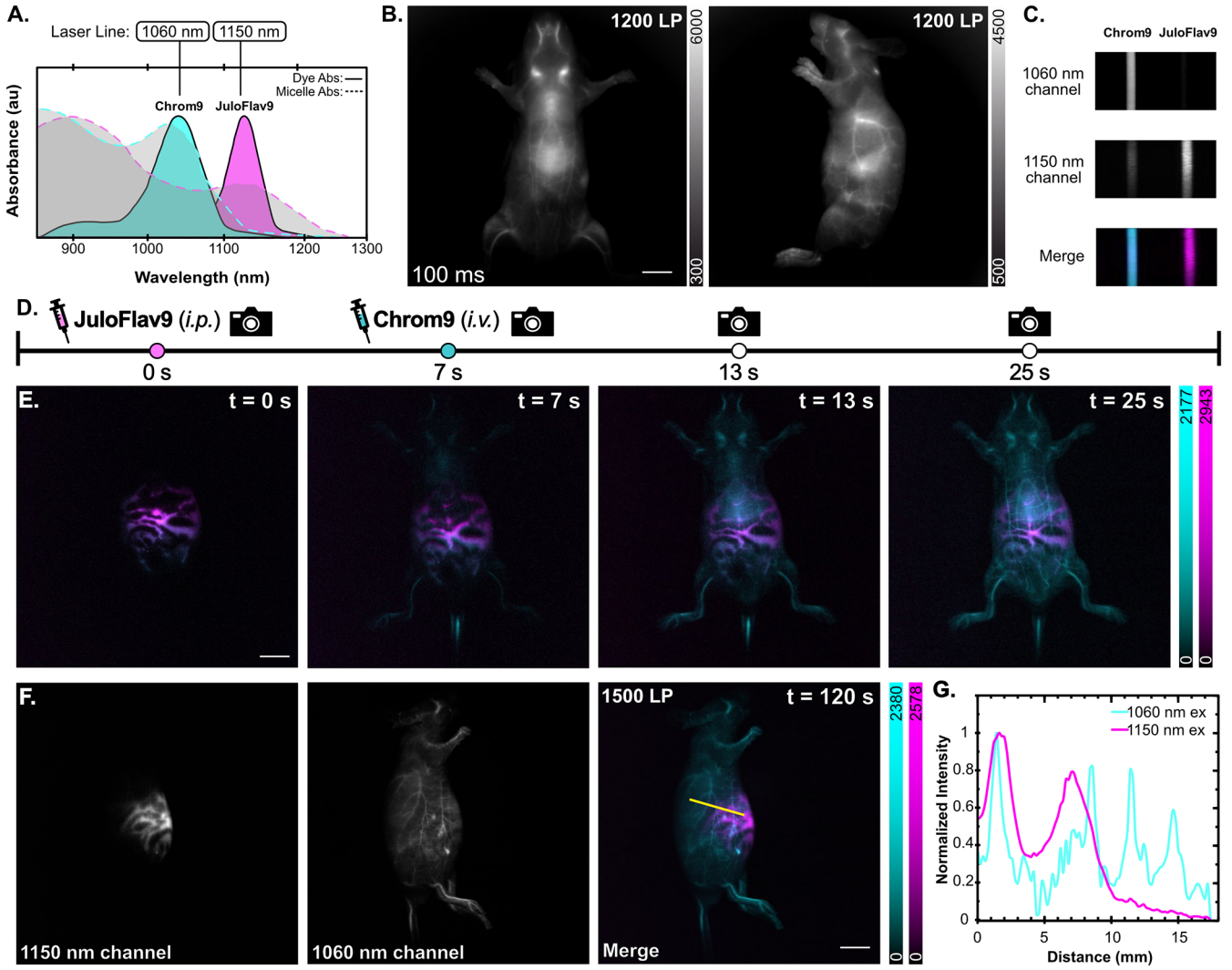

Figure 5. (A) Excitation-multiplexing strategy for two-color imaging with **1** (**Chrom9**) and **4** (**JuloFlav9**) with plotted monomer and micelle absorption. (B) Single channel imaging of **4** (**JuloFlav9**) using 1150 nm excitation; ET = 100 ms, 1200 LP, scale bar = 10 mm, power density = 50 mW cm^{-2}. (C) Two-color capillary imaging with **1** (**Chrom9**) and **4** (**JuloFlav9**) micelles. (D) Injection timeline for two-color excitation-multiplexed SWIR *in vivo* imaging. (E) Representative two-color *in vivo* imaging over the course of 25 s; ET = 20−50 ms, 1500 LP, scale bar = 10 mm. (F) Side-view 1060 and 1150 nm imaging channels and ROI, scale bar = 10 mm. (G) Plotted intensity for 1060 and 1150 nm channels from (F). Power densities for each laser were as follows: 1060 nm = 161 mW cm^{-2}; 1150 nm = 160 mW cm^{-2}. Two-color imaging with **1** (**Chrom9**) and **4** (**JuloFlav9**) was performed in duplicate (Figure S13).

biocompatible contrast agents. We injected **4** (**JuloFlav9**) into the intraperitoneal (*i.p.*) cavity of a mouse and obtained good signal with 1500 nm LP at 20 ms exposure time (Figure 5D). Next, we *i.v.* injected **1** (**Chrom9**) in the same mouse and performed excitation multiplexed two-color imaging to simultaneously visualize the vasculature and *i.p.* cavity in the high-resolution region of the SWIR (Figure 5E). We then demonstrated the orthogonal detection (Figure 5F) and subsequent quantification (Figure 5G) of signal across a ROI for both 1060 and 1150 nm channels. This is the first time excitation-based multiplexing has been successfully achieved with small molecule fluorophores with a 1500 nm LP filter. We accomplished these multiplexed experiments with respectable exposure times of 20−50 ms. Furthermore, the power densities employed in these *in vivo* experiments were well within the guidelines set by the International Commission on Non-Ionizing Radiation Protection (ICNIRP).[46]

The introduction of the 1150 nm laser also provided opportunities to extend multiplexing to five channels, a feat that was previously deemed "unlikely" for organic fluorophores.[47] By implementing the 786, 890, and 974 nm laser lines alongside the 1060 and 1150 nm lines used in the all-SWIR two-color experiments, we achieved five-color *in vivo* imaging. Previously, we developed two fluorophores, **Chrom5** and **JuloChrom5**, that could be preferentially excited by 786 and 890 nm lasers, respectively. For the 974 nm laser, there was sufficient overlap with the newly synthesized **6**, deemed **LJuloChrom7**, or **7**, deemed **LFlav7**. Through optimization of fluorophore concentration, exposure time, and/or laser power, we were able to obtain preferential excitation of each fluorophore in capillaries at their respective wavelengths (Figure S14A). We commenced a similar experiment in a mouse phantom, leading to five-color imaging of different organ chambers (Figure S14B). Notably, imaging with the

https://doi.org/10.1021/jacs.5c03673
J. Am. Chem. Soc. 2025, 147, 17384−17393

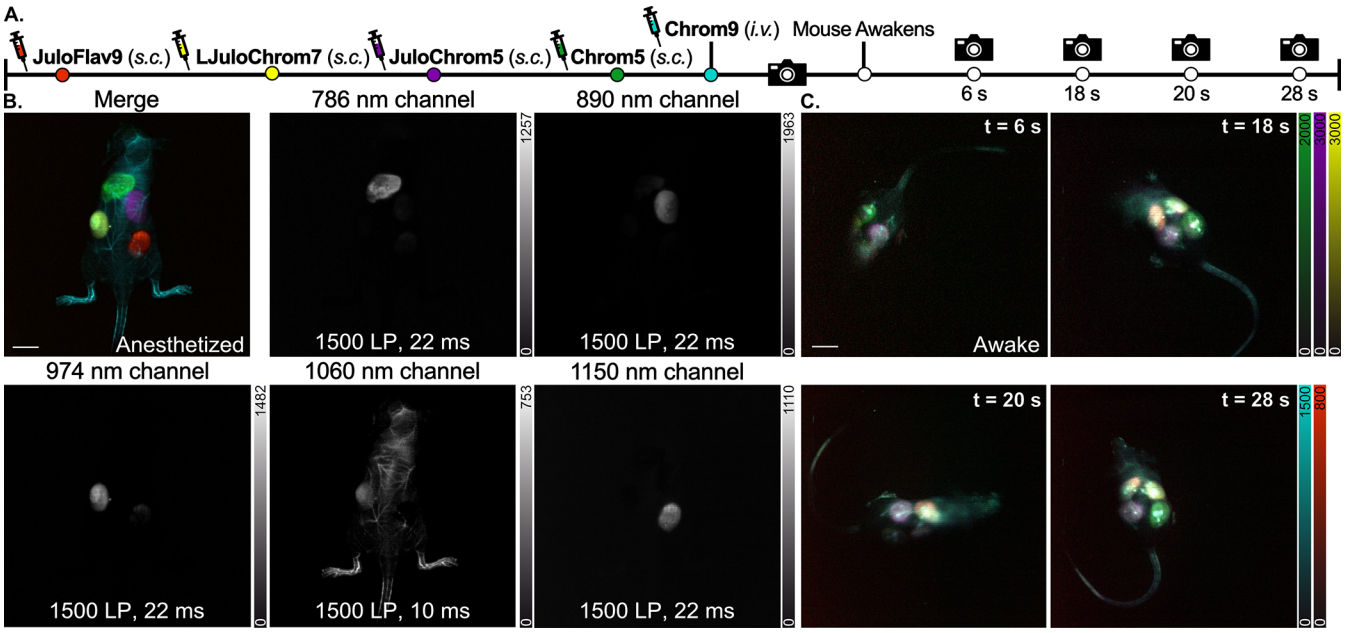

Figure 6. (A) Injection timeline for five-color multiplexed *in vivo* awake imaging. (B) After injecting **JuloFlav9**, **LJuloChrom7**, **JuloChrom5**, **Chrom5**, and **Chrom9**, five-color multiplexed imaging was performed in an anesthetized mouse; ET = 10−22 ms, 1500 LP, scale bar = 10 mm. (C) After the mouse woke up naturally, imaging was done for 28 s; ET = 10−22 ms, 1500 LP, scale bar = 10 mm. Power densities for each laser were as follows: 786 nm = 96.7 mW cm^{-2}; 890 nm = 136 mW cm^{-2}; 974 nm = 169 mW cm^{-2}; 1060 nm = 161 mW cm^{-2}; 1150 nm = 160 mW cm^{-2}.

mouse phantom was more challenging than the capillary experiments due to decreased signal from light scattering.

Taking the lessons learned from the five-color capillary and phantom experiments, we designed an *in vivo* experiment to extend those capabilities to dynamic multicolor imaging. We subcutaneously injected four dyes (1.1 nmol **JuloChrom5**, 1.2 nmol **Chrom5**, 0.7 nmol **LJuloChrom7**, 0.8 nmol **JuloFlav9**) at different spots on the back of the mouse and then intravenously injected 7.8 nmol of **Chrom9** (Figure 6A). Five-color imaging was performed on the anesthetized mouse (Figure 6B) clearly depicting five different channels using exposure times ranging from 10 to 22 ms per channel. Linear unmixing using crosstalk determined via imaging capillaries at the same concentrations and exposure times was used to separate the channels. This unmixing procedure successfully isolated all channels, though some crosstalk remained between the 974 and 1060 nm channels. We find that as we extend the multiplexing capabilities, minimizing the crosstalk with the middle channels becomes challenging as balancing contrast agent concentration with exposure times leads to contradictory results. Specifically, the increased exposure times provide crosstalk at the longer wavelengths, while increased concentration results in more significant excitation from the higher energy wavelengths. Despite a small amount of crosstalk, we were able to successfully perform a five-color, noninvasive optical imaging experiment with all small molecule probes for the first time.

Finally, we showcased the brightness of the fluorophores by imaging the animal injected with five different polymethine dyes after waking up from anesthesia. Awake animal imaging is particularly well-suited toward the fast speeds that can be achieved with optical imaging; however, the overall speed of imaging is dependent on the time it takes to collect each channel. Thus, the more channels, the more difficult it is to perform real-time imaging of awake animals. Gratifyingly, we were able to obtain satisfactory awake animal imaging with five colors (Figure 6C). We then reduced the exposure times of all five lasers down to 6 ms to enable video-rate five-color imaging (30 fps; Figure S15 and Video S2). This work sets the stage for multiplexed functional imaging of biological processes that are affected by anesthesia, such as lymphatic and neurological function.

CONCLUSIONS

The number of bright small molecule dyes capable of imaging within the higher resolution SWIR subregions of the electromagnetic spectrum is limited. In this work, we developed red-shifted nonamethine chromenylium and flavylium fluorophores that were sufficiently bright at their bandgaps. Fluorophore **1** (**Chrom9**) was shown to have bright emission above 1400 nm. The most red-shifted dye in this panel, **4** (**JuloFlav9**), allowed for imaging with excitation at 1150 nm. Upon incorporating an 1150 nm laser into an excitation multiplexed imaging setup, **Chrom9** and **JuloFlav9** were used for the first two-color SWIR excitation-multiplexed imaging with small molecule contrast agents. Notably, collection with a 1500 nm long-pass filter was possible with these bathochromically shifted fluorophores, enabling the high contrast and high depth region of the SWIR to be leveraged for multiplexed imaging. Finally, with sufficiently bright dyes, well-matched at five separate laser lines, we successfully performed real-time five color *in vivo* awake imaging with video frame rates.

The **Chrom9** and **JuloFlav9** scaffolds represent excellent core fluorophores for moving deeper into the SWIR region. Moving forward, the utility of these fluorophores can be further improved by optimizing delivery formulations, such as obtaining better monomeric properties within micelles. Within formulations, these fluorophores can be employed for visualizing and monitoring vascularization and reperfusion in real-time without the reliance of ionizing radiation. Alternatively, we have recently reported two methods to render the

https://doi.org/10.1021/jacs.5c03673
J. Am. Chem. Soc. 2025, 147, 17384−17393

heptamethine dye **Chrom7** soluble in serum/water and we expect these strategies will be applicable to the **Chrom9** scaffold.[38,48] Hydrophilic variants offer opportunities for targeted imaging and cell tracking, expanding the utility of the fluorophores. Overall, contrast agents are only as good as their imaging signal. Every endeavor toward functional probes and clinical utility starts with identifying the optimal chromophore core. **Chrom9** and **JuloFlav9** are the brightest fluorophores at their respective wavelengths and, for the first time with small molecule organic fluorophores, enable real-time imaging in the high-resolution zones of the SWIR region.

■ ASSOCIATED CONTENT

Supporting Information

The Supporting Information is available free of charge at https://pubs.acs.org/doi/10.1021/jacs.5c03673.

Additional experimental details, methods, materials, supporting figures charts and tables, and synthetic characterization of all compounds (PDF)

Single-color vasculature imaging with **Chrom9** (Video S1) (AVI)

Five-color imaging of awake mouse (Video S2) (AVI)

■ AUTHOR INFORMATION

Corresponding Author

Ellen M. Sletten − *Department of Chemistry and Biochemistry, University of California, Los Angeles, Los Angeles, California 90095, United States; California NanoSystems Institute, University of California, Los Angeles, Los Angeles, California 90095, United States;* orcid.org/0000-0002-0049-7278; Email: sletten@chem.ucla.edu

Authors

Anthony L. Spearman − *Department of Chemistry and Biochemistry, University of California, Los Angeles, Los Angeles, California 90095, United States*

Eric Y. Lin − *Department of Chemistry and Biochemistry, University of California, Los Angeles, Los Angeles, California 90095, United States*

Emily B. Mobley − *Department of Chemistry and Biochemistry, University of California, Los Angeles, Los Angeles, California 90095, United States;* orcid.org/0000-0002-4638-1123

Andriy Chmyrov − *Department of Functional Imaging in Surgical Oncology, National Center for Tumor Diseases (NCT/UCC), Dresden 01307, Germany; German Cancer Research Center (DKFZ), Heidelberg 69120, Germany; Medical Faculty and University Hospital Carl Gustav Carus, Dresden University of Technology (TUD), Dresden 01062, Germany; Helmholtz Zentrum Dresden-Rossendorf (HZDR), Dresden 01328, Germany; Helmholtz Pioneer Campus, Helmholtz Munich, Neuherberg 85764, Germany*

Bernardo A. Arús − *Department of Functional Imaging in Surgical Oncology, National Center for Tumor Diseases (NCT/UCC), Dresden 01307, Germany; German Cancer Research Center (DKFZ), Heidelberg 69120, Germany; Medical Faculty and University Hospital Carl Gustav Carus, Dresden University of Technology (TUD), Dresden 01062, Germany; Helmholtz Zentrum Dresden-Rossendorf (HZDR), Dresden 01328, Germany; Helmholtz Pioneer Campus, Helmholtz Munich, Neuherberg 85764, Germany*

Daniel W. Turner − *Department of Chemistry and Biochemistry, University of California, Los Angeles, Los Angeles, California 90095, United States*

Cesar A. Garcia − *Department of Chemistry and Biochemistry, University of California, Los Angeles, Los Angeles, California 90095, United States*

Kyle Bui − *Department of Chemistry and Biochemistry, University of California, Los Angeles, Los Angeles, California 90095, United States*

Christopher Rowlands − *Department of Bioengineering, Royal School of Mines, Imperial College London, London SW7 2AZ, United Kingdom*

Oliver T. Bruns − *Department of Functional Imaging in Surgical Oncology, National Center for Tumor Diseases (NCT/UCC), Dresden 01307, Germany; German Cancer Research Center (DKFZ), Heidelberg 69120, Germany; Medical Faculty and University Hospital Carl Gustav Carus, Dresden University of Technology (TUD), Dresden 01062, Germany; Helmholtz Zentrum Dresden-Rossendorf (HZDR), Dresden 01328, Germany; Helmholtz Pioneer Campus, Helmholtz Munich, Neuherberg 85764, Germany*

Complete contact information is available at: https://pubs.acs.org/10.1021/jacs.5c03673

Notes

The authors declare no competing financial interest.

■ ACKNOWLEDGMENTS

The authors thank the National Institute of Biological Imaging and Bioengineering (5F31EB031614-02 to A.L.S.; 1R01EB027172 to E.M.S.), the Chan Zuckerberg Initiative (2020-225707 to O.T.B., C.R., E.M.S.), the Tobacco Related Disease Research Program (T32DT4847 to E.Y.L.), UCLA Jonsson Comprehensive Cancer Center (E.B.M.), and the Foote, Tsay, and Bauer Families for fellowships to A.L.S. We would also like to thank Helmholtz Zentrum München core funding (O.T.B) National Center for Tumor Diseases (NCT) core funding (O.T.B) Deutsche Forschungsgemeinschaft (DFG) Emmy Noether program no. BR 5355/2-1 (O.T.B) German Federal Ministry of Education and Research (BMBF) project BetterView (O.T.B) Helmholtz Imaging Project grant ZT-I-PF-4-038 (O.T.B). The work was supported by shared instrumentation grants from the National Science Foundation (CHE-1048804). This work was adapted from portions of a dissertation written by A.L.S. in 2024 (Title: Elucidating design principles for chromenylium-based polymethine dyes for improved *in vivo* shortwave infrared imaging). The authors extend gratitude to Prairie Hammer (UCLA) and Quintashia Wilson (UCLA) for their assistance with characterization and Dr. Laurent Bentolila (UCLA) and the Advanced Light Microscopy/Spectroscopy Laboratory at the California NanoSystems Institute for housing the SWIR imaging setup.

■ ABBREVIATIONS

SWIR, shortwave infrared; NIR, near-infrared; VIS, visible; ICG, indocyanine green; FDA, United States Food and Drug Administration; DCM, dichloromethane; DMSO, dimethyl sulfoxide; MeOH, methanol; MeCN, acetonitrile; LP, long pass (filter); ET, exposure time; h, hour; PBS, phosphate buffered saline; i.p., intraperitoneal; i.v., intravenous; s.c., subcutaneous; fps, frames per second; ROI, region of interest;

ICNIRP, International Commission on Non-Ionizing Radiation Protection

REFERENCES

(1) Thimsen, E.; Sadtler, B.; Berezin, M. Y. Shortwave-Infrared (SWIR) Emitters for Biological Imaging: A Review of Challenges and Opportunities. *Nanophotonics* **2017**, *6*, 1043−1054.

(2) Li, C.; Chen, G.; Zhang, Y.; Wu, F.; Wang, Q. Advanced Fluorescence Imaging Technology in the Near-Infrared-II Window for Biomedical Applications. *J. Am. Chem. Soc.* **2020**, *142* (35), 14789−14804.

(3) Lei, Z.; Zhang, F. Molecular Engineering of NIR-II Fluorophores for Improved Biomedical Detection. *Angew. Chem., Int. Ed.* **2021**, *60*, 16294−16308.

(4) Ou, Y.-F.; Ren, T.-B.; Yuan, L.; Zhang, X.-B. Molecular Design of NIR-II Polymethine Fluorophores for Bioimaging and Biosensing. *Chem. Biomed. Imaging* **2023**, *1* (3), 220−233.

(5) Welsher, K.; Liu, Z.; Sherlock, S. P.; Robinson, J. T.; Chen, Z.; Daranciang, D.; Dai, H. A Route to Brightly Fluorescent Carbon Nanotubes for Near-Infrared Imaging in Mice. *Nat. Nanotechnol.* **2009**, *4* (11), 773−780.

(6) Wong, K. C. Y.; Sletten, E. M. Extending Optical Chemical Tools and Technologies to Mice by Shifting to the Shortwave Infrared Region. *Curr. Opin. Chem. Biol.* **2022**, *68*, No. 102131.

(7) Hong, G.; Diao, S.; Antaris, A. L.; Dai, H. Carbon Nanomaterials for Biological Imaging and Nanomedicinal Therapy. *Chem. Rev.* **2015**, *115* (19), 10816−10906.

(8) Tu, L.; Xu, Y.; Ouyang, Q.; Li, X.; Sun, Y. Recent Advances on Small-Molecule Fluorophores with Emission beyond 1000 nm for Better Molecular Imaging *in vivo*. *Chin. Chem. Lett.* **2019**, *30* (10), 1731−1737.

(9) Feng, Z.; Tang, T.; Wu, T.; Yu, X.; Zhang, Y.; Wang, M.; Zheng, J.; Ying, Y.; Chen, S.; Zhou, J.; Fan, X.; Zhang, D.; Li, S.; Zhang, M.; Qian, J. Perfecting and Extending the Near-Infrared Imaging Window. *Light: Sci. Appl.* **2021**, *10* (1), No. 197.

(10) Carr, J. A.; Franke, D.; Caram, J. R.; Perkinson, C. F.; Saif, M.; Askoxylakis, V.; Datta, M.; Fukumura, D.; Jain, R. K.; Bawendi, M. G.; Bruns, O. T. Shortwave Infrared Fluorescence Imaging with the Clinically Approved Near-Infrared Dye Indocyanine Green. *Proc. Natl. Acad. Sci. U.S.A.* **2018**, *115* (17), 4465−4470.

(11) Chang, B.; Chen, J.; Bao, J.; Dong, K.; Chen, S.; Cheng, Z. Design Strategies and Applications of Smart Optical Probes in the Second Near-Infrared Window. *Adv. Drug Delivery Rev.* **2023**, *192*, No. 114637.

(12) Chen, Z. H.; Wang, X.; Yang, M.; Ming, J.; Yun, B.; Zhang, L.; Wang, X.; Yu, P.; Xu, J.; Zhang, H.; Zhang, F. An Extended NIR-II Superior Imaging Window from 1500 to 1900 nm for High-Resolution *in vivo* Multiplexed Imaging Based on Lanthanide Nanocrystals. *Angew. Chem., Int. Ed.* **2023**, *62* (49), No. e202311883.

(13) Hu, Z.; Fang, C.; Li, B.; Zhang, Z.; Cao, C.; Cai, M.; Su, S.; Sun, X.; Shi, X.; Li, C.; Zhou, T.; Zhang, Y.; Chi, C.; He, P.; Xia, X.; Chen, Y.; Gambhir, S. S.; Cheng, Z.; Tian, J. First-in-Human Liver-Tumour Surgery Guided by Multispectral Fluorescence Imaging in the Visible and Near-Infrared-I/II Windows. *Nat. Biomed. Eng.* **2020**, *4* (3), 259−271.

(14) Zhao, X.; Zhang, F.; Lei, Z. The Pursuit of Polymethine Fluorophores with NIR-II Emission and High Brightness for *in vivo* Applications. *Chem. Sci.* **2022**, *13* (38), 11280−11293.

(15) Friedman, H. C.; Cosco, E. D.; Atallah, T. L.; Jia, S.; Sletten, E. M.; Caram, J. R. Establishing Design Principles for Emissive Organic SWIR Chromophores from Energy Gap Laws. *Chem* **2021**, *7* (12), 3359−3376.

(16) Ramos, P.; Friedman, H.; Li, B. Y.; Garcia, C.; Sletten, E.; Caram, J. R.; Jang, S. J. Nonadiabatic Derivative Couplings through Multiple Franck-Condon Modes Dictate the Energy Gap Law for Near and Short-Wave Infrared Dye Molecules. *J. Phys. Chem. Lett.* **2024**, *15* (7), 1802−1810.

(17) Zhang, Y.; Peng, S.; Guo, J.; Li, J.; Lu, Z.; Wu, T.; Chen, L.; Liu, W.; Feng, Z.; Zhang, M.; Qian, J. High-Definition, Video-Rate Triple-Channel NIR-II Imaging Using Shadowless Lamp Excitation and Illumination. *ACS Nano* **2025**, *19* (1), 1743−1756.

(18) Guo, J.; Zhu, Y.; Qu, Y.; Zhang, L.; Fang, M.; Xu, Z.; Wang, T.; Qin, Y.; Xu, Y.; Li, Y.; Chen, Y.; Fu, H.; Liu, X.; Liu, Y.; Liu, C.; Gao, Y.; Cui, M.; Zhou, K. Structure Tailoring of Hemicyanine Dyes for *in vivo* Shortwave Infrared Imaging. *J. Med. Chem.* **2024**, *67*, 16820−16834.

(19) Wang, T.; Chen, Y.; He, Z.; Wang, X.; Wang, S.; Zhang, F. Molecular-Based FRET Nanosensor with Dynamic Ratiometric NIR-IIb Fluorescence for Real-Time *in vivo* Imaging and Sensing. *Nano Lett.* **2023**, *23* (10), 4548−4556.

(20) Zhong, Y.; Ma, Z.; Zhu, S.; Yue, J.; Zhang, M.; Antaris, A. L.; Yuan, J.; Cui, R.; Wan, H.; Zhou, Y.; Wang, W.; Huang, N. F.; Luo, J.; Hu, Z.; Dai, H. Boosting the Down-Shifting Luminescence of Rare-Earth Nanocrystals for Biological Imaging beyond 1500 nm. *Nat. Commun.* **2017**, *8* (1), No. 737.

(21) Cosco, E. D.; Spearman, A. L.; Ramakrishnan, S.; Lingg, J. G. P.; Saccomano, M.; Pengshung, M.; Arús, B. A.; Wong, K. C. Y.; Glasl, S.; Ntziachristos, V.; Warmer, M.; McLaughlin, R. R.; Bruns, O. T.; Sletten, E. M. Shortwave Infrared Polymethine Fluorophores Matched to Excitation Lasers Enable Non-Invasive, Multicolour *in vivo* Imaging in Real Time. *Nat. Chem.* **2020**, *12* (12), 1123−1130.

(22) Cosco, E. D.; Arús, B. A.; Spearman, A. L.; Atallah, T. L.; Lim, I.; Leland, O. S.; Caram, J. R.; Bischof, T. S.; Bruns, O. T.; Sletten, E. M. Bright Chromenylium Polymethine Dyes Enable Fast, Four-Color *in vivo* Imaging with Shortwave Infrared Detection. *J. Am. Chem. Soc.* **2021**, *143* (18), 6836−6846.

(23) Arús, B. A.; Cosco, E. D.; Yiu, J.; Balba, I.; Bischof, T. S.; Sletten, E. M.; Bruns, O. T. Shortwave Infrared Fluorescence Imaging of Peripheral Organs in Awake and Freely Moving Mice. *Front. Neurosci.* **2023**, *17*, No. 1135494.

(24) Bricks, J. L.; Kachkovskii, A. D.; Slominskii, Y. L.; Gerasov, A. O.; Popov, S. V. Molecular Design of Near Infrared Polymethine Dyes: A Review. *Dyes Pigm.* **2015**, *121*, 238−255.

(25) Mostovnikov, V. A.; Rubinov, A. N.; Al'perovich, M. A.; Avdeeva, V. I.; Levkoev, I. I.; Loiko, M. M. Dependence of the Luminescence and Generation Properties of Solutions of Polymethine Dyes on Their Structure. *J. Appl. Spectrosc.* **1974**, *20* (1), 31−35.

(26) Tolbert, L. M.; Zhao, X. Beyond the Cyanine Limit: Peierls Distortion and Symmetry Collapse in a Polymethine Dye. *J. Am. Chem. Soc.* **1997**, *119* (14), 3253−3258.

(27) Bandi, V. G.; Luciano, M. P.; Saccomano, M.; Patel, N. L.; Bischof, T. S.; Lingg, J. G. P.; Tsrunchev, P. T.; Nix, M. N.; Ruehle, B.; Sanders, C.; Riffle, L.; Robinson, C. M.; Difilippantonio, S.; Kalen, J. D.; Resch-Genger, U.; Ivanic, J.; Bruns, O. T.; Schnermann, M. J. Targeted Multicolor *in vivo* Imaging over 1,000 nm Enabled by Nonamethine Cyanines. *Nat. Methods* **2022**, *19* (3), 353−358.

(28) Swamy, M. M. M.; Murai, Y.; Monde, K.; Tsuboi, S.; Jin, T. Shortwave-Infrared Fluorescent Molecular Imaging Probes Based on π-Conjugation Extended Indocyanine Green. *Bioconjugate Chem.* **2021**, *32* (8), 1541−1547.

(29) Swamy, M. M. M.; Murai, Y.; Monde, K.; Tsuboi, S.; Swamy, A. K.; Jin, T. Biocompatible and Water-Soluble Shortwave-Infrared (SWIR)-Emitting Cyanine-Based Fluorescent Probes for *in vivo* Multiplexed Molecular Imaging. *ACS Appl. Mater. Interfaces* **2024**, *16* (14), 17253−17266.

(30) Webster, S.; Padilha, L. A.; Hu, H.; Przhonska, O. V.; Hagan, D. J.; Van Stryland, E. W.; Bondar, M. V.; Davydenko, I. G.; Slominsky, Y. L.; Kachkovski, A. D. Structure and Linear Spectroscopic Properties of Near IR Polymethine Dyes. *J. Lumin.* **2008**, *128* (12), 1927−1936.

(31) Li, B.; Lu, L.; Zhao, M.; Lei, Z.; Zhang, F. An Efficient 1064 nm NIR-II Excitation Fluorescent Molecular Dye for Deep-Tissue High-Resolution Dynamic Bioimaging. *Angew. Chem., Int. Ed.* **2018**, *57* (25), 7483−7487.

(32) Pengshung, M.; Neal, P.; Atallah, T. L.; Kwon, J.; Caram, J. R.; Lopez, S. A.; Sletten, E. M. Silicon Incorporation in Polymethine Dyes. *Chem. Commun.* **2020**, *56*, 6110−6113.

https://doi.org/10.1021/jacs.5c03673
J. Am. Chem. Soc. 2025, 147, 17384−17393

(33) Li, B.; Zhao, M.; Zhang, F. Rational Design of Near-Infrared-II Organic Molecular Dyes for Bioimaging and Biosensing. *ACS Mater. Lett.* **2020**, *2* (8), 905−917.
(34) Lei, Z.; Sun, C.; Pei, P.; Wang, S.; Li, D.; Zhang, X.; Zhang, F. Stable, Wavelength-Tunable Fluorescent Dyes in the NIR-II Region for *in vivo* High-Contrast Bioimaging and Multiplexed Biosensing. *Angew. Chem., Int. Ed.* **2019**, *58*, 8166−9171.
(35) East, A. K.; Lee, M. C.; Smaga, L. P.; Jiang, C.; Mallojjala, S. C.; Hirschi, J. S.; Chan, J. Synthesis of Silicon-Substituted Hemicyanines for Multimodal SWIR Imaging. *Org. Lett.* **2022**, *24* (46), 8509−8513.
(36) Pengshung, M.; Li, J.; Mukadum, F.; Lopez, S. A.; Sletten, E. M. Photophysical Tuning of Shortwave Infrared Flavylium Heptamethine Dyes via Substituent Placement. *Org. Lett.* **2020**, *22* (15), 6150−6154.
(37) Pengshung, M.; Cosco, E. D.; Zhang, Z.; Sletten, E. M. Counterion Pairing Effects on a Flavylium Heptamethine Dye. *Photochem. Photobiol.* **2022**, *98* (2), 303−310.
(38) Jia, S.; Lin, E. Y.; Mobley, E. B.; Lim, I.; Guo, L.; Kallepu, S.; Low, P. S.; Sletten, E. M. Water-Soluble Chromenylium Dyes for Shortwave Infrared Imaging in Mice. *Chem* **2023**, *9* (12), 3648−3665.
(39) Matikonda, S. S.; Helmerich, D. A.; Meub, M.; Beliu, G.; Kollmannsberger, P.; Greer, A.; Sauer, M.; Schnermann, M. J. Defining the Basis of Cyanine Phototruncation Enables a New Approach to Single-Molecule Localization Microscopy. *ACS Cent. Sci.* **2021**, *7* (7), 1144−1155.
(40) Okoročenkova, J.; Filgas, J.; Khan, N. M.; Slavíček, P.; Klán, P. Thermal Truncation of Heptamethine Cyanine Dyes. *J. Am. Chem. Soc.* **2024**, *146* (29), 19768−19781.
(41) Vahdani, A.; Moemeni, M.; Holmes, D.; Lunt, R. R.; Jackson, J. E.; Borhan, B. Mechanistic Insight into the Thermal "Blueing" of Cyanine Dyes. *J. Am. Chem. Soc.* **2024**, *146* (29), 19756−19767.
(42) Roy, S.; Bag, N.; Bardhan, S.; Hasan, I.; Guo, B. Recent Progress in NIR-II Fluorescence Imaging-Guided Drug Delivery for Cancer Theranostics. *Adv. Drug Delivery Rev.* **2023**, *197*, No. 114821.
(43) Pascal, S.; Haefele, A.; Monnereau, C.; Charaf-Eddin, A.; Jacquemin, D.; Le Guennic, B.; Andraud, C.; Maury, O. Expanding the Polymethine Paradigm: Evidence for the Contribution of a Bis-Dipolar Electronic Structure. *J. Phys. Chem. A* **2014**, *118* (23), 4038−4047.
(44) Janeková, H.; Friedman, H. C.; Russo, M.; Zyberaj, M.; Ahmed, T.; Hua, A. S.; Sica, A. V.; Caram, J. R.; Šťacko, P. Deuteration of Heptamethine Cyanine Dyes Enhances Their Emission Efficacy. *Chem. Commun.* **2024**, *60* (8), 1000−1003.
(45) Cosco, E. D.; Caram, J. R.; Bruns, O. T.; Franke, D.; Day, R. A.; Farr, E. P.; Bawendi, M. G.; Sletten, E. M. Flavylium Polymethine Fluorophores for Near- and Shortwave Infrared Imaging. *Angew. Chem., Int. Ed.* **2017**, *56* (42), 13126−13129.
(46) Ziegelberger, G.; Croft, R.; Feychting, M.; Green, A. C.; Hirata, A.; d'Inzeo, G.; Jokela, K.; Loughran, S.; Marino, C.; Miller, S.; Oftedal, G.; Okuno, T.; van Rongen, E.; Röösli, M.; Sienkiewicz, Z.; Tattersall, J.; Watanabe, S. Guidelines for Limiting Exposure to Electromagnetic Fields (100 kHz to 300 GHz). *Health Phys.* **2020**, *118* (5), 483−524.
(47) Kobayashi, H.; Hama, Y.; Koyama, Y.; Barrett, T.; Regino, C. A. S.; Urano, Y.; Choyke, P. L. Simultaneous Multicolor Imaging of Five Different Lymphatic Basins Using Quantum Dots. *Nano Lett.* **2007**, *7* (6), 1711−1716.
(48) Mobley, E. B.; Lin, E. Y.; Sletten, E. M. Chromenylium Star Polymers: Merging Water Solubility and Stealth Properties with Shortwave Infrared Emissive Fluorophores. *ACS Cent. Sci.* **2025**, *11*, 208−218.

https://doi.org/10.1021/jacs.5c03673
J. Am. Chem. Soc. 2025, 147, 17384−17393